

HOMO-LUMO, ESP, NBO, and Lipophilic Character Analyses of Flutriafol and Its Trifluorinated Analogue

Sümeyya Serin¹ 

¹Inönü University, Scientific and Technological Research Center, Malatya

Geliş Tarihi / Received Date: 25.11.2022

Kabul Tarihi / Accepted Date: 09.05.2023

Abstract

This current study focuses on the exploration of the impacts of OH/F isosteric replacement using computational chemistry methods. To this end, Density Functional Theory (DFT) calculations at B3LYP/6-311++G (d, p) level of theory were carried out on flutriafol, a broad-spectrum fungicide, and its trifluorinated analogue. The reflections of OH/F isosteric replacement on frontier molecular orbital energies, reactivity behaviors, electrostatic surface properties and intramolecular interactions were investigated. Also, one of the important consequences of isosteric and bioisosteric replacements is the modification in lipophilic character, which is a remarkable parameter in many respects. Therefore, lipophilic character evaluations were performed for mentioned molecules using SwissADME and Molinspiration software.

Keywords: DFT, flutriafol, isosterism, lipophilicity

Flutriafol ve Triflorlanmış Analoğunun HOMO-LUMO, ESP, NBO ve Lipofilik Karakter Analizleri

Öz

Bu mevcut çalışma, hesaplamalı kimya yöntemleri kullanılarak OH/F izosterik yer değiştirmesinin etkilerinin araştırılmasına odaklanmaktadır. Bu amaçla, geniş spektrumlu bir fungusit olan flutriafol ve triflorlanmış analoğu üzerinde B3LYP/6-311++G (d, p) teori düzeyinde Yoğunluk Fonksiyonel Teori (YFT) hesaplamaları yapılmıştır. OH/F izosterik yer değiştirmesinin sınır moleküler orbital enerjilerine, reaktivite davranışlarına, elektrostatik yüzey özelliklerine ve moleküleri etkileşimlerine yansımaları incelenmiştir. Ayrıca izosterik ve biyoizosterik süstitüsyonların önemli sonuçlarından biri de birçok açıdan dikkate değer bir parametre olan lipofilik karakterdeki değişimdir. Bu nedenle, söz konusu moleküller için SwissADME ve Molinspiration yazılımı kullanılarak lipofilik karakter değerlendirmeleri yapılmıştır.

Anahtar kelimeler: YFT, flutriafol, izosterizm, lipofilisite

Introduction

Fungicides, which are important members of the pesticide class, are widely used in agriculture to prevent and/or directly eliminate fungal infections (Beyer et al., 2006; Wise et al., 2019). Inorganic substances such as lime, copper, sulfur, and mercury compounds were among the first used fungicides. Depending on whether the fungicides are used consciously, regularly and adequately, some fungicides, like other pesticides, may cause resistance in fungi. Over the years, a great deal of substances with broadly varying chemical components has been developed and used as fungicides (Lu et al., 2014; Pasteris et al., 2016). Conazole fungicides are frequently used both agriculturally and pharmaceutically. They include potent fungicidal stereoisomers that inhibit ergosterol biosynthesis in fungi by preventing 14 α -demethylation. They are synthetic substances that can be divided into two groups as imidazole and triazole (Faro, 2010; Lewis et al., 2016). Flutriafol (1) is a commercial triazole fungicide. Flutriafol and its derivatives are known to be effective in controlling numerous diseases affecting various fruits, trees and cereal crops. On the other hand, the widespread use of (1) poses a danger to the aquatic ecosystem (Zhang et al., 2015). Therefore, there was a need for new agrochemical candidates that could exhibit the characteristics of an effective fungicide. These characteristics can be listed as low toxicity to mammals, low ecotoxicity, high penetration rate, and limited biodegradation. Fluorine substitution is a significant tool in the exploration for the optimum candidate in modern plant protection in terms of effectiveness, environmental and user friendliness (Jeschke, 2004). The significance of fluorine substitution in agrochemical industry can be attributed to the physicochemical properties resulting from the incorporation of fluorine and fluorine groups into bioactive molecules (Filler, 1986). Accordingly, the number of active pesticide products containing fluorine substituents has increased over the years (Jeschke, 2004).

It is an important feature that the fluorine atom can imitate hydrogen atom or hydroxy group due to its van der Waals radius similarity (F: 1.47 Å; H: 1.20 Å; OH: 1.40 Å). Therefore, it is concluded that physicochemical changes that may occur as a result of isosteric substitution of fluorine with H or OH may positively affect bioactivity. For this purpose, trifluorinated analogue (2) was obtained as a result of incorporation of fluorine atom into broad-spectrum fungicide flutriafol and it was determined that it showed similar activity (Jeschke, 2004).

Flutriafol is a well-known molecule. Its fungicidal effects have been studied in many studies (Bhuiyan et al., 2014; Cotterill, 1993; Karaoglanidis et al., 2003). In addition, enantiomeric determination studies were carried out using chromatographic methods (Shuang et al., 2021; Ying et al., 2009; Zhang et al., 2015). On the other hand, no quantum chemical analysis study on flutriafol and/or its trifluorinated analogue has been found, except for study on kinetics and mechanisms of \cdot OH-mediated mineralization (Liu et al., 2017). In the study by Liu et al, quantum chemical computations along with electrochemical experiments were used to elucidate the \cdot OH-mediated mechanisms of degradation of (1) in detail. Based on DFT computations, the optimal \cdot OH-mediated mineralization mechanism of (1) was reported, and an array of intermediates were observed accumulated in the degradation process. Whereas, as a result of the literature search, HOMO-LUMO, ESP, and NBO analyzes were found for neither (1) nor (2) molecules. Especially, the evaluation of lipophilic characters of mentioned molecules both numerically and visually by using SwissADME and Molinspiration software highlights the originality of this study.

Herein, a theoretical study has been carried out for flutriafol (1) and its trifluorinated analogue (2) (Figure 1). In this study, it is aimed to investigate the effects of isosteric replacement of fluorine by using quantum chemical methods. In this context, calculations were performed on compounds (1) and (2) using the DFT/B3LYP/6-311++G (d, p) methodology. The reactivities of the molecules were examined by calculating quantum chemical descriptors. Frontier molecular orbital energies, electrostatic surface properties, and intramolecular interactions were compared. In addition, *in silico* examination results of lipophilic character properties and physicochemical magnitudes of both molecules were interpreted.

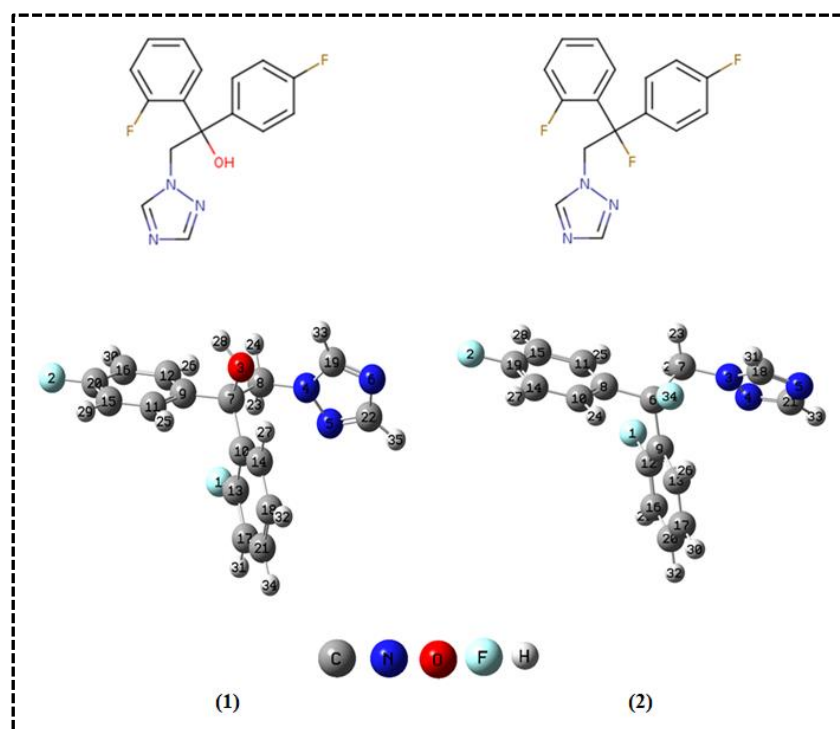


Figure 1. Chemical Representations and DFT-Optimized Molecular Structures of (1) and (2)

Computational Methods and Theory

Geometry optimization calculations of (1) and (2) were performed at DFT level by using the GAUSSIAN 16 package program in the gas phase (Frisch et al., 2016). In optimization and frequency computations, Becke, three-parameter, Lee-Yang-Parr (B3LYP) functional was used with 6-311++G (d, p) split-valence triple zeta basis set that implicates both polarization and diffuse functions (Becke, 1993; Lee et al., 1988). The optimized structures are presented in Figure 1. The absence of imaginary frequency for all calculations confirmed optimized structures. Also, HOMO-LUMO diagrams and ESP maps of the mentioned molecules were visualized using Gauss View 6 software (Dennington et al., 2006). SwissADME software (Daina et al., 2017) was used to estimate the basic physicochemical and lipophilicity characteristics of the mentioned molecules. Besides, molecular lipophilicity potential (MLP) and topological polar surface area (TPSA) maps of studied molecules were visualized in Molinspiration Galaxy 3D Structure Generator v2018.01 beta (Gaillard et al., 1994).

FMO theory analysis was performed to evaluate reactivity behaviors of (1) and (2). All the quantum chemical descriptors were computed with Koopmans Theorem according to the following equations (Koopmans, 1934; Parr, 1999; Parr & Pearson, 1983; Pearson, 1986; Perdew & Levy, 1983; Perdew et al., 1982):

$$\text{Ionization Energy (I)} \quad I = -E_{HOMO} \quad (1)$$

$$\text{Electron Affinity (A)} \quad A = -E_{LUMO} \quad (2)$$

$$\text{Energy Gap } (\Delta E) \quad \Delta E = E_{LUMO} - E_{HOMO} \quad (3)$$

$$\text{Chemical Potential } (\mu) \quad \mu = -\frac{I + A}{2} \quad (4)$$

$$\text{Chemical Hardness } (\eta) \quad \eta = \frac{I - A}{2} \quad (5)$$

$$\text{Electronegativity } (\chi) \quad \chi = \frac{I + A}{2} \quad (6)$$

$$\text{Electrophilicity index } (\omega) \quad \omega = \frac{\mu^2}{2\eta} \quad (7)$$

Further, NBO analyses of (1) and (2) were performed to interpret donor and acceptor orbitals interactions, hybridizations and stabilization energy estimations. Hereof, it is an influential and often used method. NBO analyses were carried out with NBO 3.1 program (Glendening et al., 1998) integrated into Gaussian program by using B3LYP/6-311++G (d, p) method. Donor-acceptor orbitals interactions were calculated using second order Fock matrix (Reed et al., 1988; Weinhold et al., 2016). The equation stated below was used to calculate the stabilization energy values.

$$E^{(2)} = \Delta E_{ij} = qi \left[\frac{(F_{ij})^2}{(\epsilon_j - \epsilon_i)} \right] \quad (8)$$

The terms in the equation (8) and their explanations are as follows: ϵ_i and ϵ_j : diagonal element, donor and acceptor orbital energies, F_{ij} : Off diagonal Fock matrix, q_i : Donor orbital occupancy, $E^{(2)}$: Stabilization energy.

Result and Discussion

HOMO-LUMO and ESP Analyses

Estimating the energy values of the HOMO (Highest Occupied Molecular Orbital) and the LUMO (Lowest Unoccupied Molecular Orbital) of a particular molecule and determining their locations play an important role in its reactivity analysis. Figure 2 displays the 3D HOMO-LUMO diagrams with their energy values corresponding to the vacuum environment. It is clear that for both molecules the HOMOs are distributed almost throughout the molecule. Only for the molecule (2) the density on the triazole ring is slightly less than for the molecule (1). On the other hand, in both molecules, LUMOs appear to be predominantly concentrated on regions outside the triazole ring. It is noteworthy that the density on the ortho-fluorophenyl group in (2) molecule decreased compared to (1).

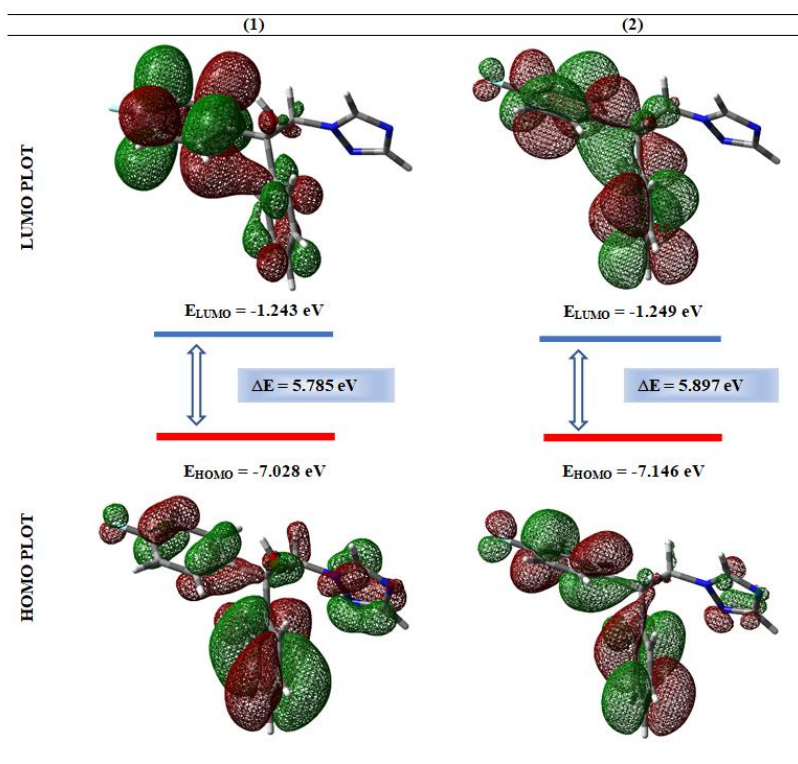


Figure 2. FMO Plots of (1) and (2)

In computational chemistry, it is a very effective strategy to utilize some vital quantum chemical descriptors as well as the energy gap (ΔE), calculated from the difference of HOMO and LUMO energies, to make reactivity predictions on a particular molecule. HOMO-LUMO energy values are obtained directly from Gaussian output files. Quantum chemical reactivity descriptors (QCRD) calculated using these energy values are presented in Table 1. As demonstrated in Table 1, the energy gap values for compounds (1) and (2) were calculated as 5.785 eV and 5.897 eV, respectively. It is noteworthy that isosteric fluorine substitution increased the HOMO-LUMO gap. Considering the results, the fact that (2) has higher ionization energy (7.146 eV) and electron affinity (1.249 eV) values shows that it is more dominant than (1) as both electron-donor and electron-acceptor. In addition, (2) exhibits stronger electronegativity (4.197 eV).

Table 1. The Calculated QCRDs of (1) and (2) in eV

	E_{HOMO}	E_{LUMO}	ΔE	η	μ	χ	ω
(1)	-7.028	-1.243	5.785	2.892	-4.135	4.135	2.957
(2)	-7.146	-1.249	5.897	2.948	-4.197	4.197	2.988

Furthermore, MEP, ESP, and contour maps of both molecules are displayed in Figure 3. Electrostatic surface property analysis is a crucial approach in order to interpret electrophilic and nucleophilic sites for chemical reactions and hydrogen bond interactions (Murray & Politzer, 2011; Murray & Sen, 1996). The nucleophilic locations are specified by blue, whereas the electrophilic locations are specified by red on three-dimensional charge distribution of MEP maps. The ranges of MEP and ESP were calculated for both molecules in vacuum environment as ± 0.05890 a.u. and ± 0.01284 a.u. respectively. As demonstrated in MEP maps, for molecules (1) and (2), the negative regions are located around nitrogen atoms of triazole ring. On the other hand, for the molecule (1), the deepest blue region is concentrated around the hydrogen atom bound to the oxygen. For molecule (2), the light blue regions are concentrated around the carbons and hydrogens of the phenyl ring and the CH₂ group. Blue color reflects positive regions. Similarly, while the negative ESPs are concentrated

more over the nitrogen atoms of triazole ring, and are reflected as yellowish blobs, the positive ESPs are concentrated on the rest of the molecules. It is evident that positive surfaces increase in molecule (2).

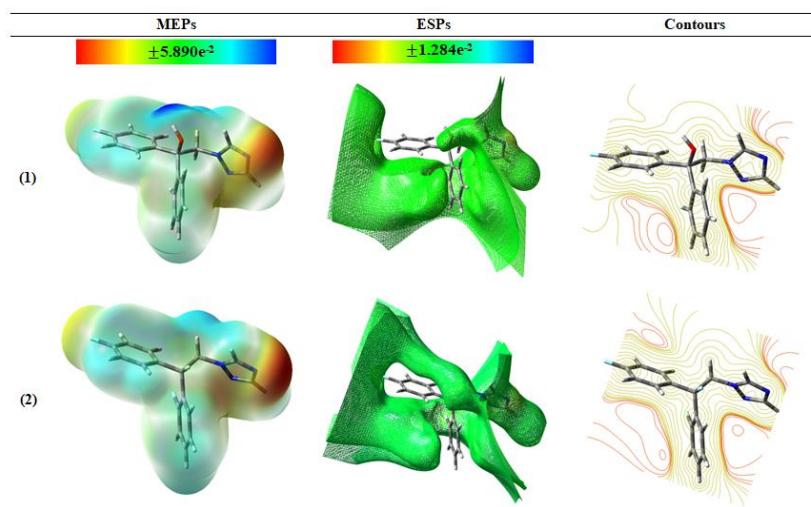


Figure 3. MEP, ESP, and Contour Maps of (1) and (2)

NBO Analysis

In this section of study, NBO analyses of (1) and (2) were examined. Table 2 comprises a summa of donor-acceptor orbital interactions and occupancy values, as well as stabilization energies calculated according to equation (8). Interactions with stabilization energy of 10 kcal/mol and above are taken into account. According to NBO analysis, for (1), the Lewis natural bond orbitals define 97.459% (valence Lewis of 96.477% and core of 99.959%.) of the total electron density. The remaining non-Lewis density was found 2.541% (valence non-Lewis of 2.328% and Rydberg non-Lewis of 0.213%). For (2), the Lewis natural bond orbitals define 97.467% (valence Lewis of 96.488% and core of 99.959%.) of the total electron density. The remaining non-Lewis density was found 2.533% (valence non-Lewis of 2.325% and Rydberg non-Lewis of 0.208%).

Table 2. Second-Order Perturbation Analysis Results of Fock Matrix in NBO Basis for (1) and (2)

	Donor(i)	ED _i /e	Acceptor(j)	ED _j /e	E ⁽²⁾ kcal/mol	E(j)-E(i)/a.u	F(i,j)/a.u
(1)	π N5-C22	1.88866	π* N6-C19	0.37804	10.42	0.32	0.055
	π N6-C19	1.82152	π* N5-C22	0.34562	30.99	0.31	0.092
	π C9-C12	1.67482	π* C11-C15	0.31932	21.26	0.29	0.070
			π* C16-C20	0.36029	18.39	0.28	0.065
	π C10-C14	1.67189	π* C13-C17	0.36177	23.12	0.28	0.072
			π* C18-C21	0.33164	18.52	0.29	0.065
	π C11-C15	1.67988	π* C9-C12	0.35917	18.60	0.29	0.066
			π* C16-C20	0.36029	23.06	0.28	0.072
	π C13-C17	1.66415	π* C10-C14	0.35586	19.04	0.30	0.068
			π* C18-C21	0.33164	20.46	0.30	0.070
	π C16-C20	1.65828	π* C9-C12	0.35917	21.21	0.30	0.071
	π C18-C21	1.66658	π* C11-C15	0.31932	18.20	0.30	0.066
			π* C10-C14	0.35586	21.97	0.28	0.071
			π* C13-C17	0.36177	19.66	0.27	0.066
	LP (3) F1	1.92862	π* C13-C17	0.36177	17.19	0.44	0.084
	LP (3) F2	1.92537	π* C16-C20	0.36029	18.40	0.43	0.086
LP (1) N4	1.53868	π* N5-C22	0.34562	25.50	0.28	0.078	
		π* N6-C19	0.37804	51.08	0.28	0.109	
	Donor(i)	ED _i /e	Acceptor(j)	ED _j /e	E ⁽²⁾ kcal/mol	E(j)-E(i)/a.u	F(i,j)/a.u
(2)	π N4-C21	1.88838	π* N5-C18	0.37485	10.47	0.32	0.055
	π N5-C18	1.82235	π* N4-C21	0.34280	30.90	0.31	0.091
	π C8-C11	1.67347	π* C10-C14	0.32012	21.42	0.29	0.070
			π* C15-C19	0.36319	18.54	0.28	0.065
	π C9-C13	1.67342	π* C12-C16	0.36142	22.92	0.28	0.072
			π* C17-C20	0.33040	18.45	0.29	0.065
	π C10-C14	1.67694	π* C8-C11	0.35922	18.66	0.29	0.066
			π* C15-C19	0.36319	23.43	0.28	0.073
	π C12-C16	1.66289	π* C9-C13	0.36123	19.15	0.30	0.068
			π* C17-C20	0.33040	20.34	0.30	0.070
	π C15-C19	1.65753	π* C8-C11	0.35922	21.33	0.30	0.071
			π* C10-C14	0.32012	18.14	0.30	0.066
	π C17-C20	1.66214	π* C9-C13	0.36123	22.27	0.28	0.071
			π* C12-C16	0.36142	19.84	0.27	0.066
	LP (3) F1	1.92888	π* C12-C16	0.36142	17.09	0.44	0.084
	LP (3) F2	1.92573	π* C15-C19	0.36319	18.33	0.43	0.086
LP (1) N3	1.54168	π* N4-C21	0.34280	25.32	0.28	0.078	
		π* N5-C18	0.37485	50.58	0.28	0.108	

As indicated in Table 2, there are fourteen π - π^* and four (lone pair) LP- π^* interactions that contribute to the stabilization of each molecule. It is observed that the number, kind and magnitude of high-energy intramolecular interactions are quite similar. The energies of π - π^* interactions alter between 10.52 kcal/mol and 31.80 kcal/mol while the energies of LP- π^* interactions are between 18.14 kcal/mol and 52.48 kcal/mol. A high stabilization energy value indicates that the interaction between the specified orbitals is intense. That is, the greater the propensity to donate, the greater the degree of conjugation of the entire system. According to Table 2, the highest stabilization energy for (1) was found to belong to the LP (1) N4 ($ED_i = 1.53868e$) \rightarrow π^* N6-C19 ($ED_j = 0.37804e$) interaction and its value was calculated as 51.08 kcal/mol. Similarly, the highest stabilization energy for (2) corresponded to the LP (1) N3 ($ED_i = 1.54168e$) \rightarrow π^* N5-C18 ($ED_j = 0.37485e$) interaction and its value was calculated as 50.58 kcal/mol.

Lipophilic Character Analysis

It is of great importance to investigate the physicochemical properties of agrochemical candidates in order to determine their toxicity, biodegradability and bioaccumulation tendencies. One of the most

important physicochemical properties is lipophilicity. Estimations of n-octanol/water partition coefficient ($\log P_{ow}$), which allows lipophilic character appraisals, are considerable in the field of agrochemical industry, environmental monitoring, and pharmacology (Dolowy et al., 2014; Skyner et al., 2015). It is known that the presence of fluorine substituents in bioactive molecules increases lipophilicity. In this way, fluorine substituents can affect the in vivo uptake and transport of the active components (Jeschke, 2004). Therefore, in this part of the study, the physicochemical effects resulting from the substitution of the tertiary hydroxyl group in the biologically active (1) with fluorine atom were examined in silico. To this end, SwissADME and Molinspiration software were utilized. Both web tools are freely accessible and easy to use. In Figure 4, bioavailability radar diagrams related to the physicochemical properties of (1) and (2) with BOILED-Egg presentations were given. The pink colored region in the radar diagram symbolizes the appropriate physicochemical area for oral bioavailability (Dhiabi et al., 2023). According to the radar diagram, (1) and (2) are in the pink area except for the saturation value. The bioavailability score of each molecule was computed as 55%. In addition, BOILED-egg graphical method (Figure 4) is used in order to predict passive human intestinal absorption (HIA, oval white part) and Blood-Brain Barrier (BBB, yellow yolk-like sphere) permeability. The remaining gray area indicates low absorption and limited brain penetration (Bakchi et al., 2022). The studied molecules are seen as red hollow spheres on the yellow region. Red color represents PGP- (P-glycoprotein, efflux capability of the molecules through the biological membranes).

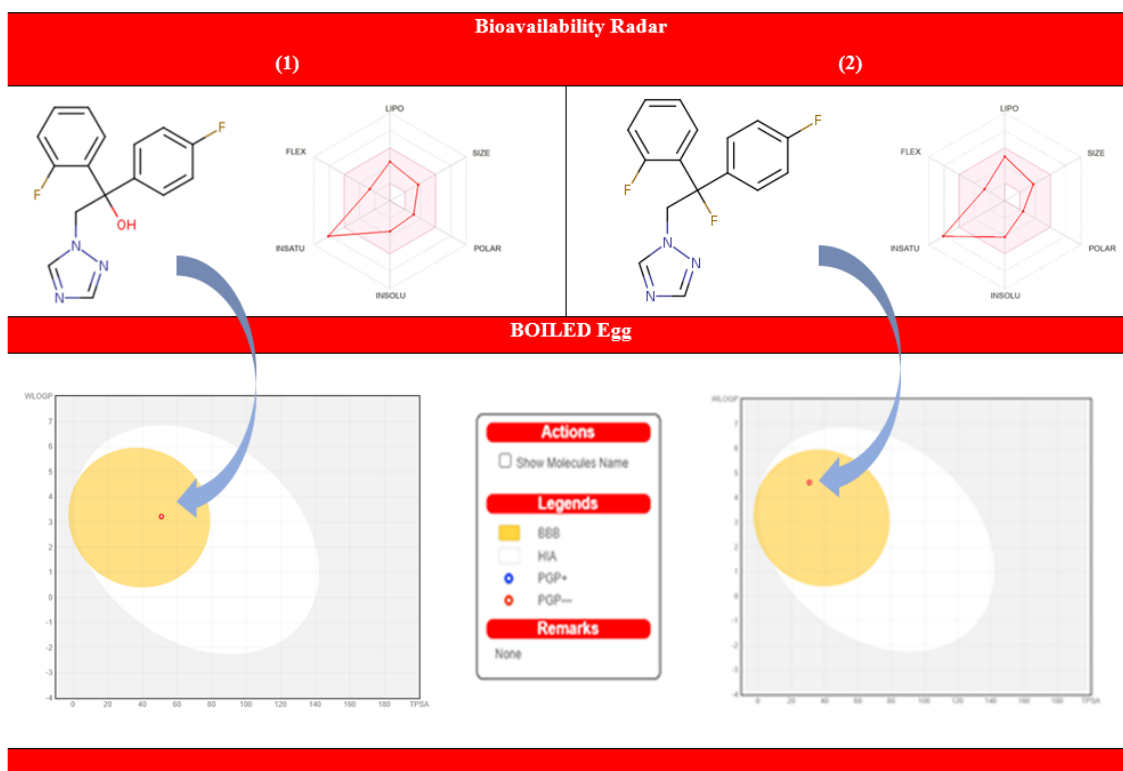


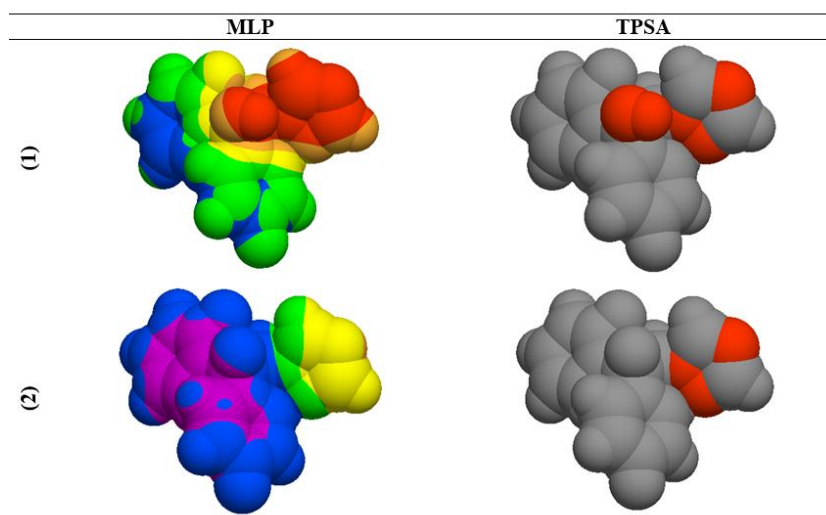
Figure 4. BOILED-Egg Representations and Bioavailability Radar Diagrams of (1) and (2)

Table 3 contains numerical estimates of the physicochemical and lipophilic properties of molecules (1) and (2). Although the physicochemical properties were calculated to be similar for both molecules, the change in topological polar surface area (TPSA) value is remarkable. As expected, the TPSA value decreased from 50.94 Å² to 30.71 Å² as a result of the substitution of the OH group with fluorine atom. This is supported by the polar surface area maps obtained via Molinspiration software and illustrated in Figure 5. In TPSA maps, gray color represents non-polar regions and red color represents polar Regions. Therefore, it is evident that the red-colored regions decreased in the transition from (1) to (2).

Table 3. Estimations of Physicochemical Properties and LogP_{ow} Values for (1) and (2)

Physicochemical Properties	(1)	(2)	Lipophilicity LogP	(1)	(2)
Molecular weight	301.29 g/mol	303.28 g/mol	iLOGP	1.99	2.23
Num. of heavy atoms	22	22	XLOGP3	2.30	3.33
Num. of arom. heavy atoms	17	17	WLOGP	3.22	4.62
Num. of rotatable bonds	4	4	MLOGP	3.00	3.97
Num. of H bond acceptors	5	5	SILICOS-IT	2.93	3.83
Num. of H bond donors	1	0	Consensus	2.69	3.60
Molar Refractivity	76.03	74.92			
TPSA	50.94 Å ²	30.71 Å ²			

In lipophilic character analysis, iLOGP, XLOGP3, WLOGP, MLOGP, and SILICOS-IT predictive models are taken into account via SwissADME software. The arithmetic average of whole models is presented as consensus logP_{ow}. Estimations and consensus logP_{ow} values for (1) and (2) are listed in Table 3. As demonstrated in Table 3, the consensus logP_{ow} value for (1) was calculated as 2.69, which is in good agreement with the value given in the literature for flutriafol (logP_{ow} = 2.30) (Benfenati et al., 2003). On the other hand, for (2), the consensus logP_{ow} value was calculated as 3.60. Since fluorine substitution is known to increase lipophilicity, the result obtained is quite reasonable. As with polar surface area assessment, lipophilicity results can be supplemented with molecular lipophilicity potential (MLP) maps obtained via Molinspiration software, as shown in Figure 5. Color codes were also used in MLP maps. Orange/red regions define hydrophilic surfaces while violet/blue regions define the most lipophilic surfaces. Last, regions coded in yellow/green point out intermediate lipophilic surfaces. It is clearly seen that the blue and violet zones representing the lipophilic surfaces are more intense in compound (2). On the other side, in compound (1), the red and orange hydrophilic regions originating from the hydroxyl group are more dominant. Therefore, (2) is expected to be more lipophilic than (1), as expressed in MLP maps. At this point, it is obvious that both SwissADME and Molinspiration analysis results support each other.

**Figure 5.** 3D CPK View of PSA and MLP Maps of (1) and (2)

Conclusions

Isosterism or bioisosterism is a widely used method in the design of new active molecules both in the pharmaceutical sciences and in the agrochemical industry. In these time-consuming and expensive design processes, it is an effective approach to predict the bioactivity and metabolism behaviors of drug and agrochemical candidates utilizing computational chemistry methods. In this paper, results of DFT/B3LYP/ 6-311++G (d, p) computations made for (1) and (2) have been reported. The theoretical findings of OH/F isosteric replacement are as follows: i) isosteric fluorine substitution

increased the HOMO-LUMO gap; ii) It is observed that the number, kind and magnitude of high-energy intramolecular interactions are quite similar for (1) and (2). The interactions with the highest stabilization energy are LP (1) N4 \rightarrow π^* N6-C19 (51.08 kcal/mol) and LP (1) N3 \rightarrow π^* N5-C18 (50.58 kcal/mol) interactions; iii) In silico analysis highlighted the meaningful changes in TPSA and logPow values. SwissADME and Molinspiration analysis results were found to support each other.

Acknowledgment

The numerical calculations reported in this paper were partially performed at TUBITAK ULAKBIM, High Performance and Grid Computing Center (TRUBA resources).

Author Contribution

Sümeyya Serin, performed the data collection, theoretical analysis, and writing of the article.

Ethic

There are no ethical issues with the publication of this article.

Conflict of Interest

The author declares that there is no conflict of interest.

ORCID

Sümeyya Serin  <https://orcid.org/0000-0002-4637-1734>

References

- Becke, A. D. (1993). A new mixing of Hartree–Fock and local density-functional theories. *Journal of Chemical Physics*, 98, 1372–1377. <https://doi.org/10.1063/1.464304>
- Becke, A. D. (1993). Density-functional thermochemistry. III. The role of exact exchange. *Journal of Chemical Physics*, 98, 5648–5652. <https://doi.org/10.1063/1.464913>
- Benfenati, E., Gini, G., Piclin, N., Roncaglioni, A., & Varı, M. R. (2003). Predicting logP of pesticides using different software. *Chemosphere*, 53, 1155–1164. [https://doi.org/10.1016/S0045-6535\(03\)00609-X](https://doi.org/10.1016/S0045-6535(03)00609-X)
- Beyer, M., Klix, M. B., Klink, H., J. A., & Verreet, J. A. (2006). Quantifying the effects of previous crop, tillage, cultivar and triazole fungicides on the deoxynivalenol content of wheat grain—a review. *Journal of Plant Diseases and Plant Protection*, 113, 241–246. <https://doi.org/10.1007/BF03356188>
- Bhuiyan, S.A., Croft, B.J. & Tucker, G.R. (2014). Efficacy of the fungicide flutriafol for the control of pineapple sett rot of sugarcane in Australia. *Australasian Plant Pathology*, 43, 413–419. <https://doi.org/10.1007/s13313-014-0282-y>
- Bulti Bakchi, B., Krishna, A. D., Sreecharan, E., Ganesh, V. B. J., Niharika, M., Maharshi, S., Puttagunta, S. B., Sigalapalli, D. K., Bhandare, R. R., & Shaik, A. B. (2022). An overview on applications of SwissADME web tool in the design and development of anticancer, antitubercular and antimicrobial agents: A medicinal chemist's perspective. *Journal of Molecular Structure*, 1259, 132712. <https://doi.org/10.1016/j.molstruc.2022.132712>
- Cotterill, P. J. (1993). Effect of flutriafol on saprophytic survival and growth of *Rhizoctonia solani* (AG-8). *Australasian Plant Pathology*, 22(2), 53-57. <https://doi.org/10.1071/APP9930053>
- Daina, A., Michielin, O., Zoete, V. (2017). SwissADME: A free web tool to evaluate pharmacokinetics, drug-likeness and medicinal chemistry friendliness of small molecules. *Scientific Reports*, 7(1), 1-13. <https://doi.org/10.1038/srep42717>.

- Dennington, R., Keith, T. A., & Millam, J. M. (2016). GaussView, Version 6. Semichem Inc., Shawnee Mission.
- Dhiabi, M., Bouattour, A., Fakhfakh, M., Abid, S., Paquin, L., Robert, T., Bach, S., Bazureau, J. P., & Ammar, H. (2023). Practical approach to N -benzyl derivatives of 2-amino-8-methoxy-4 H-chromene-3-carbonitrile by reductive amination: Exploration of their effects against protein kinases and in silico ADME profiling. *Journal of Molecular Structure* 1274, 134319, <https://doi.org/10.1016/j.molstruc.2022.134319>
- Dolowy, M., Miszczyk, M., & Pyka, A. (2014). Application of various methods to determine the lipophilicity parameters of the selected urea pesticides as predictors of their bioaccumulation. *Journal of Environmental Science and Health, Part B*, 49, 730-737. <https://doi.org/10.1080/03601234.2014.929481>
- Faro, L. R. (2010). Neurotoxic effects of triazole fungicides on nigrostriatal dopaminergic neurotransmission. In Odile Carisse (Ed.), *Fungicides* (pp. 405-420). InTech. <https://doi.org/10.5772/13109>
- Filler, R. (1986). Biologically-active fluorochemicals. *Journal of Fluorine Chemistry*, 33, 1-4. [https://doi.org/10.1016/S0022-1139\(00\)85281-1](https://doi.org/10.1016/S0022-1139(00)85281-1)
- Frisch, M. J.; Trucks, G. W.; Schlegel, H. B.; Scuseria, G. E.; Robb, M. A.; Cheeseman, J. R.; Scalmani, G.; Barone, V.; Petersson, G. A.; Nakatsuji, H.; Li, X.; Caricato, M.; Marenich, A. V.; Bloino, J.; Janesko, B. G.; Gomperts, R.; Mennucci, B.; Hratchian, H. P.; Ortiz, J. V.; Izmaylov, A. F...Fox, D. J. (2016). Gaussian 16, Rev B.01. Wallingford CT.
- Gaillard, P., Carrupt, P.A., Testa, B., & Boudon, A. (1994). Molecular lipophilicity potential, a tool in 3D QSAR: Method and applications. *Journal of Computer-Aided Molecular Design*, 8, 83-96. <https://doi.org/10.1007/BF00119860>
- Glendening, E. D., Reed, A. E., Carpenter, J. E., & Weinhold, F. (1998). NBO Version 3.1, TCI, University of Wisconsin.
- Jeschke, P. (2004). The unique role of fluorine in the design of active ingredients for modern crop protection. *ChemBioChem*, 5, 570-589. <https://doi.org/10.1002/cbic.200300833>
- Karaoglanidis, G. S., Karadimos, D. A., Ioannidis, P. M. (2003). Detection of resistance to sterol demethylation-inhibiting (DMI) fungicides in cercospora beticola and efficacy of control of resistant and sensitive strains with flutriafol. *Phytoparasitica* 31(4), 373-380. <https://doi.org/10.1007/BF02979809>
- Koopmans, T. (1934). Über die zuordnung von wellenfunktionen und eigenwerten zu den einzelnen elektronen eines atoms. *Physica*, 1(6), 104-113. [https://doi.org/10.1016/S0031-8914\(34\)90011-2](https://doi.org/10.1016/S0031-8914(34)90011-2)
- Lee, C., Yang, W., & Parr, R. G. (1988). Development of the Colle-Salvetti correlation-energy formula into a functional of the electron density. *Physical Review B*, 37, 785-789. <https://doi.org/10.1103/PhysRevB.37.785>
- Lewis, K., Tzilivakis, J., Warner, D., & Green, A. (2016). An international database for pesticide risk assessments and management, *Human and Ecological Risk Assessment: An International Journal*, 22, 1050-1064. <https://doi.org/10.1080/10807039.2015.1133242>
- Liu, S., Zhou, X., Han, W., Li, J., Sun, X., Shen, J., & Wang, L. (2017). Theoretical and experimental insights into the OH-mediated mineralization mechanism of flutriafol. *Electrochimica Acta*, 235, 223-232. <https://doi.org/10.1016/j.electacta.2017.03.062>
- Lu, A., Wang, J., Liu, T., Han, J., Li, Y., Su, M., Chen, J., Zhang, H., L. Wang, L., & Wang, Q. (2014). Small changes result in large differences: Discovery of (-)-incrustoporin derivatives as novel antiviral

- and antifungal agents. *Journal of Agricultural and Food Chemistry*, 62, 8799–8807. <https://doi.org/10.1021/jf503060k>.
- Molinspiration Cheminformatics (1986). Cheminformatics Software Tools. Retrieved September 25, 2022 from <https://www.molinspiration.com>
- Murray, J. S., & Sen, K. (1996). *Molecular electrostatic potentials: concepts and applications*. Elsevier.
- Murray, J. S., & Politzer, P. (2011). The Electrostatic potential: An overview, *Wiley Interdisciplinary Reviews: Computational Molecular Science*, 1, 153–163, <https://doi.org/10.1002/wcms.19>
- Parr, R. G., & Pearson, R. G. (1983). Absolute hardness: companion parameter to absolute electronegativity. *Journal of the American Chemical Society*, 105, 7512-7516. <https://doi.org/10.1021/ja00364a005>
- Parr, R. G. (1999). Electrophilicity index. *Journal of the American Chemical Society*, 121, 1922-1924. <https://doi.org/10.1021/ja983494x>
- Pasteris, R. J., Hanagan, M. A., J.J. Bisaha, J. J., Finkelstein, B. L., Hoffman, L. E., Gregory, V., Andreassi, J. L., Sweigard, J. A., Klyashchitsky, B. A., Henry, Y. T., & Berger, R. A. (2016). Discovery of oxathiapiroprolin, a new oomycete fungicide that targets an oxysterol binding protein. *Bioorganic & Medicinal Chemistry*, 24, 354–361. <https://doi.org/10.1016/j.bmc.2015.07.064>
- Pearson, R. G. (1986). Absolute electronegativity and hardness correlated with molecular orbital theory. *Proceedings of the National Academy of Sciences of the United States of America*, 83(22), 8440-8441. <https://doi.org/10.1073/pnas.83.22.8440>
- Perdew, J. P., Parr, R. G., Levy, M., & Balduz, J. L. (1982). Density-Functional Theory for fractional particle number: derivative discontinuities of the energy. *Physical Review Letters*, 49, 1691. <https://doi.org/10.1103/PhysRevLett.49.1691>
- Perdew, J. P., & Levy, M. (1983). Physical content of the exact Kohn-Sham orbital energies: band gaps and derivative discontinuities. *Physical Review Letters*, 151(20), 1884-1887. <https://doi.org/10.1103/PhysRevLett.51.1884>
- Reed, A. E., Curtiss, L.A., & Weinhold, F. (1988). Intermolecular interactions from a natural bond orbital, donor-acceptor viewpoint. *Chemical Reviews*, 88(6), 899-926. <https://doi.org/10.1021/cr00088a005>
- Shuang, Y., Zhang, T., Zhong, H., & Li, L. (2021). Simultaneous enantiomeric determination of multiple triazole fungicides in fruits and vegetables by chiral liquid chromatography/tandem mass spectrometry on a bridged bis(β -cyclodextrin)-bonded chiral stationary phase. *Food Chemistry*, 345, 128842. <https://doi.org/10.1016/j.foodchem.2020.128842>
- Skyner, R. E., McDonagh, J. L., Groom, C. R., van Mourik, T., & Mitchell, J. B. O. (2015). A review of methods for the calculation of solution free energies and the modelling of systems in solution. *Physical Chemistry Chemical Physics*, 17, 6174-6191. <https://doi.org/10.1039/C5CP00288E>
- Weinhold, F., Landis, C. R., Glendening, E. D. (2016). What is NBO analysis and how is it useful? *International Reviews in Physical Chemistry*, 35(3), 399-440. <https://doi.org/10.1080/0144235X.2016.1192262>
- Wise, K. A., Smith, D., Freije, A., Mueller, D. S., Kandel, Y., Allen, T., Bradley, C. A., Byamukama, E., Chilvers, M., Faske, T., Friskop, A., Hollier, C., Ziems, T. A. J., & Tenuta, A. (2019). Meta-analysis of yield response of foliar fungicide-treated hybrid corn in the United States and Ontario, Canada. *PLoS One*. 14(6), 0217510. <https://doi.org/10.1371/journal.pone.0217510>
- Ying, Z., Ling, L., Kunde, L., Xinping, Z., & Weiping, L. (2009), Enantiomer separation of triazole fungicides by high-performance liquid chromatography. *Chirality*, 21, 421-427. <https://doi.org/10.1002/chir.20607>

- Zhang, Q., Hua, X-d., Shi, H-y., Liu, J-s., Tian, M-m., & Wang, M-h. (2015). Enantioselective bioactivity, acute toxicity and dissipation in vegetables of the chiral triazole fungicide flutriafol. *Journal of Hazardous Materials*, 284, 65–72. <https://doi.org/10.1016/j.jhazmat.2014.10.033>
- Zhang, Q., Hua, X., & Yang, Y. (2015). Stereoselective degradation of flutriafol and tebuconazole in grape. *Environmental Science and Pollution Research*, 22, 4350–4358. <https://doi.org/10.1007/s11356-014-3673-2>